See-Through Walls: Motion Tracking Using Variance-Based Radio Tomography Networks

Joey Wilson and Neal Patwari, *Member*, *IEEE*

Abstract—This paper presents a new method for imaging, localizing, and tracking motion behind walls in real time. The method takes advantage of the motion-induced variance of received signal strength measurements made in a wireless peer-to-peer network. Using a multipath channel model, we show that the signal strength on a wireless link is largely dependent on the power contained in multipath components that travel through space containing moving objects. A statistical model relating variance to spatial locations of movement is presented and used as a framework for the estimation of a motion image. From the motion image, the Kalman filter is applied to recursively track the coordinates of a moving target. Experimental results for a 34-node through-wall imaging and tracking system over a 780 square foot area are presented.

Index Terms—Wireless networks, sensors, tracking, through-wall surveillance.

✦

1 INTRODUCTION

THIS paper explores a method for tracking the location of a person or object behind walls, without the need for an electronic device to be attached to the target. The technology is an extension of "radio tomographic imaging" [1], which is so-called because of its analogy to medical tomographic imaging methods. We call this extension *variance-based radio tomographic imaging* (VRTI), since it uses the signal strength variance caused by moving objects within a wireless network. The general field of locating people or objects when they don't carry a device is also called "device-free passive localization" [2] in contrast to technologies like active radio frequency identification (RFID) which only locate objects that carry a radio transmitter.

For context-aware systems, a user's context includes the locations of people in the nearby environment [3]. Typically, location aware systems require the participation of people who must wear tags to be located and identified [4]. We envision applications in which requiring participation is not possible. For example, emergency responders, miltary forces, or police arrive at a scene where entry into a building is potentially dangerous. They deploy radio sensors around (and potentially on top of) the building area, either by throwing or launching them, or dropping them while moving around the building. The nodes immediately form a network and self-localize, perhaps using information about the size and shape of the building from a database (e.g., Google maps) and some known-location coordinates (e.g., using GPS). Then, nodes begin to transmit, making signal strength measurements on links which cross the building or area of interest. The "received signal strength" (RSS) measurements

of each link are transmitted back to a base station and used to estimate the positions of moving people and objects within the building. Based on these inputs, the context aware system can aid decisions about how to focus responders' efforts.

Radio tomography provides life-saving benefits for emergency responders, police, and military personnel arriving at potentially dangerous situations. Many correctional and law enforcement officers are injured each year because they lack the ability to detect and track offenders through building walls [5]. By showing the locations of people within a building during hostage situations, building fires, or other emergencies, radio tomography can help law enforcement and emergency responders to know where they should focus their attention.

This paper explores the use of radio tomography in highly obstructed areas for the purpose of tracking moving objects through walls. First, a review of previous work and related research is summarized in Section 2. In Section 3, we address a fundamentally different method for the use of RSS measurements which we call VRTI. When a moving object affects the amplitude or phase of one or more multipath components over time, the phasor sum of all multipath at the receiver experiences changes, and higher RSS variance is observed. The amount of RSS variance relates to the physical location of motion, and an image representing motion is estimated using measurements from many links in the wireless network.

We briefly review the Kalman filter and apply it in Section 4 to track the location of a moving object or person. In Section 5, experimental results demonstrate the use of RSS variance to locate a moving object on the inside of a building. This section also quantifies the accuracy of localization by comparing known movement paths with those estimated by the VRTI tracking system. We show that the VRTI system can track the location of an experimenter behind walls with approximately two feet average error for this experiment.

Finally, Section 6 discusses some possibilities for future research. Advances in wireless protocols, antenna design, and physical layer modeling will bring improvements to VRTI through-wall tracking.

- *The authors are with the Sensing and Processing Across Networks (SPAN) Lab, University of Utah, 50 South Campus Drive, Rm. 3280 MEB, Salt Lake City, UT 84108.*
  E-mail: joey.wilson@utah.edu, npatwari@ece.utah.edu.

2 RELATED RESEARCH

Previous work shows that changes in link path losses can be used to accurately estimate an image of the attenuation field, that is, a spatial plot of attenuation per unit area [1]. Experimental tests show that in an unobstructed area surrounded by a network of nodes, the estimated image displayed the positions of people in the area.

Indoor radio channel characterization research demonstrates that objects moving near wireless communication links cause variance in RSS measurements [6]. This knowledge has been applied to detect and characterize motion of network nodes and moving objects in the network environment [7]. Polarization techniques have also been used to detect motion [8]. These studies focus mostly on detection and velocity characterization of movement, but do not attempt to localize the movement as the work presented in this paper does.

Youssef, Mah, and Agrawala [2] demonstrated that variance of RSS on a number of WiFi links in an indoor WLAN can be used to 1) detect if motion is occurring within a wireless network and 2) localize the moving object based on a manually trained lookup. In many situations, however, manual training is not possible since it can take a significant amount of time and access to the area being tracked is restricted.

Real-time location systems (RTLS) are based on a technology that uses electronic tags for locating objects. For logistics purposes in large facilities, commercial real-time location systems are deployed by installing infrastructure in the building and attaching active RFID tags to each object to be tracked. RTLS systems are not useful in most emergency operations, however, since they require setup inside of a building prior to system use. Further, RTLS systems cannot locate people or objects which do not have an RFID tag. In emergencies, an operation cannot rely on an adversary wearing a tag to be located. Thus, tag-based localization methods are insufficient for most emergency and security applications.

An alternate tag-free localization technology is ultra-wideband (UWB) through-wall imaging (TWI) (also called through-the-wall surveillance). In radar-based TWI, a wideband phased array steers a beam across space and measures the delay of the reflection response, estimating a bearing and distance to each target. Through-wall radar imaging has garnered significant interest in recent years [9], [10], [11], [12], [13], for both static imaging and motion detection. Commercial products include Cambridge Consultants' Prism 200 [14] and Camero Tech's Xaver 800 [15], and are prohibitively expensive for most applications, on the order of US $100,000 per unit. These products are accurate close to the device, but inherently suffer from accuracy and noise issues at long range due to monostatic radar losses. In free space at distance d, radar systems measure power proportional to $1/d^4$, in comparison to $1/d^2$ for radio transmission systems.

Radio tomography takes a fundamentally different approach from traditional TWI systems by using large networks of sensors. While initial attempts [16] have allowed 2-4 high-complexity devices to collaborate in TWI, our research investigates the use of tens or hundreds of collaborating nodes to simultaneously image a larger area than possible with a single through-wall radar. RTI's imaging capability increases as $\mathcal{O}(N^2)$ for N sensors; thus, large networks, rather than highly capable nodes, lead to improved imaging and tracking capabilities.

Multistatic radar research has also developed technologies called multiple-input multiple-output (MIMO) radar. These technologies also use distributed devices, perhaps without phase synchronization, in order to measure radar scattering [17]. The use of many distributed antennas is a type of spatial diversity for a radar system which can then avoid nulls in the radar cross-section (RCS) of a scattering object as a function of scattering angle [18].

MIMO radar is a complementary technology to radio tomography. While MIMO radar measures scattering of the transmitted signal by the object of interest, radio tomography methods are based on measurements of transmission through a medium. Integration of the two modalities is beyond the scope of this paper, but is perhaps a promising direction for future research.

3 VARIANCE-BASED RADIO TOMOGRAPHIC IMAGING

In this section, we introduce and justify a model which relates motion in spatial voxels to the variance of signal strength measured on the links of a wireless network. In particular, we justify the assumption of a linear model when motion is sparse, and describe the limits on the validity of such a model.

3.1 Measurement Model

The goal of a VRTI system is to use a vector $\mathbf{s}$ of RSS variance measurements on M links in a wireless network to determine an image vector $\mathbf{x}$ that describes the presence of motion occurring within N voxels of a physical space. We first describe the image vector, then specifically define RSS, and discuss RSS variance.

The image vector $\mathbf{x}$ is a representation of motion occurring within each spatial voxel of the network area, with jth element given by

$$x(j) = \begin{cases} 1, & \text{if motion occurs in voxel } j, \\ 0, & \text{otherwise.} \end{cases} \quad (1)$$

What we call the RSS is actually a measure of the received power in decibels. In a multipath environment, a wireless signal travels along many paths from transmitter to receiver. Each path has associated with it an amplitude and phase, and the received signal is a summation of each incoming multipath component. The complex baseband voltage for a continuous-wave (CW) signal measured at a receiver is expressed as [19]

$$\tilde{V} = \nu + \sum_{i=1}^{L} V_i \exp(j\Phi_i), \quad (2)$$

where ν is the additive noise, V_i is the magnitude, and Φ_i is the phase of the ith multipath component (wave) impinging on the receiver antenna. The received power is thus $\|\tilde{V}\|^2$, and so the RSS, denoted R_{dB}, is given as $R_{dB} = 10 \log_{10} \|\tilde{V}\|^2$.

The RSS variance vector **s** contains for each link a measure of the variance of R_{dB}. In Section 3.2, we show how this variance has a linear relationship with the total power in affected multipath. Then in Section 3.3, we argue that this total affected power has a linear relationship with **x**, for the case of sparse motion. In sum, we justify the following linear model. We approximate $\text{Var}[R_{dB}]$ as a linear combination of the movement occurring in each voxel, weighted by the amount of variance that motion in that particular voxel causes on the link's RSS

$$\text{Var}[R_{dB}] = \sum_j w_j x(j) + n, \tag{3}$$

where n is measurement noise and modeling error, and w_j is the variance caused by movement in voxel j. For all links, we have

$$\mathbf{s} = \mathbf{W}\mathbf{x} + \mathbf{n}, \tag{4}$$

where **W** is an $M \times N$ matrix representing the variance weighting for each pixel and link, and **n** is a $M \times 1$ noise vector.

3.2   Variance and Total Affected Power

In this section, we argue that the RSS variance, $\text{Var}[R_{dB}]$, and the total affected power have a linear relationship. First, we define affected power. We classify each multipath as either *affected* or *static*: A multipath i is described as affected if its amplitude and/or phase change randomly as a result of the current position of people and/or objects in the channel, or static if it is not. We denote $\mathcal{A}(\mathbf{x})$ to be the indices of the affected multipath given the motion described in **x**. Then we define the total affected power, $T_{AP}(\mathbf{x})$, as

$$T_{AP}(\mathbf{x}) = \sum_{i \in \mathcal{A}(\mathbf{x})} |V_i|^2. \tag{5}$$

We show that T_{AP} has a linear relationship with $\text{Var}[R_{dB}]$ for a wide range of $\text{Var}[R_{dB}]$.

Rearranging the multipath in (2) into affected and static contributions

$$\tilde{V} = \nu + \sum_{i \notin \mathcal{A}(\mathbf{x})} V_i \exp(j\Phi_i) + \sum_{i \in \mathcal{A}(\mathbf{x})} V_i \exp(j\Phi_i). \tag{6}$$

The sum of static multipaths do not change, and thus, we can rewrite (6) as

$$\tilde{V} = \bar{V} \exp(j\bar{\Phi}) + \sum_{i \in \mathcal{A}(\mathbf{x})} V_i \exp(j\Phi_i) + \nu, \tag{7}$$

where $\bar{V}$ and $\bar{\Phi}$ are the magnitude and phase angle of $\sum_{i \notin \mathcal{A}(\mathbf{x})} V_i \exp(j\Phi_i)$, respectively. We consider the V_i and Φ_i for affected multipath to be random.

It is well known in the wireless communications literature [20], [21] that $|\tilde{V}|$, as it is given in (7), is well represented as a Ricean random variable. The voltage $\bar{V}e^{j\bar{\Phi}}$ is analogous to the specular signal in a Ricean channel, while the remaining terms are the diffuse signal components. The K factor of the Ricean distribution for $|\tilde{V}|$ is defined as
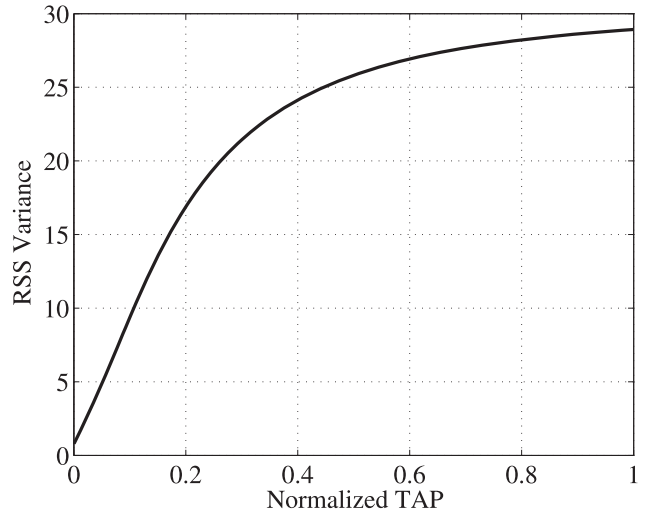

Fig. 1. The variance of RSS versus normalized TAP, $T_{AP}(\mathbf{x})/\bar{V}^2$, for $\sigma_\nu^2/\bar{V}^2 = 0.01$.

$$K = \frac{\bar{V}^2}{2\sigma^2} = \frac{\bar{V}^2}{2[\sigma_\nu^2 + T_{AP}(\mathbf{x})]} = \frac{1}{2}\left[\frac{\sigma_\nu^2}{\bar{V}^2} + \frac{T_{AP}(\mathbf{x})}{\bar{V}^2}\right]^{-1}, \tag{8}$$

where $\sigma^2 = \sigma_\nu^2 + T_{AP}(\mathbf{x})$ is the power in the affected power and noise, and $T_{AP}(\mathbf{x})$ is defined in (5). We refer to $T_{AP}(\mathbf{x})/\bar{V}^2$ as the normalized total affected power (normalized TAP).

Moreover, we have a known relationship between the variance of RSS and K. Since $R_{dB} = 10 \log_{10} \|\tilde{V}\|^2$ and $|\tilde{V}|$ is Ricean, R_{dB} has the log-Ricean pdf. The variance of R_{dB} is calculated numerically as a function of K. Note that for constant K, the scale of σ^2 and $\bar{V}^2$ do not change $\text{Var}[R_{dB}]$. Combining the numerically calculated relationship between $\text{Var}[R_{dB}]$ and K, and (8), we plot in Fig. 1 the functional dependence of $\text{Var}[R_{dB}]$ on normalized TAP.

As seen in Fig. 1, the variance of RSS is linearly related to normalized TAP for normalized TAP less than 0.25. That is, when the total power affected by a Person's motion is less than 25 percent of the total static power in the link, the variance is linear with normalized TAP. For through-wall imaging, the power affected by the motion inside of the building is typically low, because multipath which penetrate two external walls to enter and exit the building are low in power compared to multipath which diffract around the building's exterior.

For high normalized TAP, the variance strictly increases, so motion can be detected using VRTI, but the nonlinearities make the linear model, and thus the proposed image estimator, less accurate. In this case, we note that moving objects are also likely to cause a reduction in the mean received power, because they typically cause some shadowing of the affected multipath. As a result, shadowing-based RTI may be a better approach than variance-based RTI when most of the multipath power is affected, that is, when all links are LOS, but not in through-wall deployments.

In short, RSS variance has a linear relationship with total affected power, over the most important range of normalized TAP for purposes of variance-based RTI.

3.3   Total Affected Power and Motion

In this section, we argue that for sparse motion, the total affected power is approximately linear in **x**. Assume that

multipath component i travels through a subset of space $\mathcal{S}_i$. This subset $\mathcal{S}_i$ might be some narrow volume around the line tracing its path from the transmitter to receiver, for example. We assume that a path i is affected due to object motion in voxel j centered at $\mathbf{z}_j$ if $\mathbf{z}_j \in \mathcal{S}_i$, then path i is affected, i.e.,

$$\mathcal{A}(\mathbf{x}) = \{i : x(j) > 0 \ \cap \ \mathbf{z}_j \in \mathcal{S}_i, \quad \text{for some } j\}.$$

Note that $x(j)$ is nonnegative as given in (1). Now consider two motion images, $\mathbf{x}_1$ and $\mathbf{x}_2$. The affected multipath in the sum motion image, $\mathbf{x} = \mathbf{x}_1 + \mathbf{x}_2$, is given by

$$\begin{aligned} \mathcal{A}(\mathbf{x}) &= \{i : x_1(j) + x_2(j) > 0 \ \cap \ \mathbf{z}_j \in \mathcal{S}_i, \quad \text{for some } j\} \\ &= \mathcal{A}(\mathbf{x}_1) \cup \mathcal{A}(\mathbf{x}_2). \end{aligned} \quad (9)$$

Then, the total affected power, as defined in (5), due to the sum of the motion vectors is

$$\begin{aligned} T_{AP}(\mathbf{x}) &= \sum_{i \in \mathcal{A}(\mathbf{x}_1) \cup \mathcal{A}(\mathbf{x}_2)} |V_i|^2 = \sum_{i \in \mathcal{A}(\mathbf{x}_1)} |V_i|^2 + \sum_{i \in \mathcal{A}(\mathbf{x}_2)} |V_i|^2 \\ &- \sum_{i \in \mathcal{A}(\mathbf{x}_1) \cap \mathcal{A}(\mathbf{x}_2)} |V_i|^2. \end{aligned} \quad (10)$$

This intersection $\mathcal{A}(\mathbf{x}_1) \cap \mathcal{A}(\mathbf{x}_2)$ is the set of multipaths affected by both motion images $\mathbf{x}_1$ and $\mathbf{x}_2$.

Now, let $\mathbf{x}_1$ and $\mathbf{x}_2$ be sparse motion images with motion only in voxels j_1 and j_2, respectively. Then,

$$\mathcal{A}(\mathbf{x}_1) \cap \mathcal{A}(\mathbf{x}_2) = \{i : \mathbf{z}_{j_1} \in \mathcal{S}_i \ \cap \ \mathbf{z}_{j_2} \in \mathcal{S}_i\},$$

that is, a multipath which crosses through both voxels j_1 and j_2. We argue that for close voxels, i.e., $\|\mathbf{z}_{j_1} - \mathbf{z}_{j_2}\|$ small, there may be a multipath which crosses through both voxels. However, for voxels j_1 and j_2 far apart, there will be relatively few multipath components which cross through both voxels, compared to the multipath which crosses through only one. In this latter case, (10) becomes

$$T_{AP}(\mathbf{x}_1 + \mathbf{x}_2) \approx \sum_{i \in \mathcal{A}(\mathbf{x}_1)} |V_i|^2 + \sum_{i \in \mathcal{A}(\mathbf{x}_2)} |V_i|^2. \quad (11)$$

In general, when the nonzero motion voxels in $\mathbf{x}_1$ and $\mathbf{x}_2$ are relatively distant, the approximation in (11) is valid. This model, in combination with the linearity between $T_{AP}(\mathbf{x})$ and the RSS variance, justifies approximating $\mathbf{s}$ as a linear transformation of $\mathbf{x}$ as given in (4).

3.4 Elliptical Weight Model

If knowledge of an environment were available, one could estimate the variance weights w_j for each link. Perhaps calibration measurements or ray tracing techniques could aid in estimation of the linear transformation $\mathbf{W}$. For time-critical emergency operations, one cannot expect to obtain floor plans and interior arrangements of the building. With no site-specific information, we require a statistical model that describes the contribution of motion in each pixel to a link's variance.

One such statistical model has been described for link shadowing is the normalized elliptical model [1], [22]. Consider an ellipsoid with foci at the transmitter and receiver locations. The excess path length of multipath contained within this ellipsoid must be less than or equal to a constant. Excess path length is defined as the path length

of the multipath minus the path length of the line-of-sight component. As described in previous sections, the variance of a link's RSS is highly related to the power contained in the mulipath components affected by motion. With this reasoning, we make the assumption that motion occurring on voxels within an ellipsoid will contribute significantly to a link's RSS variance, while motion in voxels outside will not. This is a binary quantization, but provides a simple, single-parameter spatial model. We note that measurements in [23], [24] also show elliptical-shaped areas in which motion causes high variance.

The variance weight for each voxel decreases as the distance between two nodes increases. As the link gets longer, the amount of power in the changing multipath components is decreased along with the link's RSS variance. Many models for distance weighting could be applied for images with varying qualities, but our empirical tests have indicated that dividing the variance weighting by the root of the link distance generates images that contain a balance of contrast and noise-reduction. The weighting is described mathematically as

$$[W]_{l,j} = \frac{1}{\sqrt{d_l}} \begin{cases} \psi, & \text{if } d_{lj}(1) + d_{lj}(2) < d_l + \lambda, \\ 0, & \text{otherwise,} \end{cases} \quad (12)$$

where d_l is the distance between the two nodes, $d_{lj}(1)$ and $d_{lj}(2)$ are the distances from the center of voxel j to the two respective node locations on link l, ψ is a constant scaling factor used to normalize the image, and λ is a tunable parameter describing the excess path length included in the ellipsoid.

The normalized ellipse weight model is certainly an approximation, but experimental data has shown its effectiveness for VRTI, as will be shown in Section 5. Future work will use theoretical arguments and extensive measurements to refine the statistical models of RSS variance as a function of location.

3.5 Process Sampling, Buffering, and Variance Estimation

In this paper, we assume that the link signal strength process is sampled at a constant time period T_s, resulting in the discrete-time signal for link l:

$$R_l[k] = R_{dB_l}(kT_s), \quad (13)$$

where $R_{dB_l}(kT_s)$ is the RSS measurement in dB at time kT_s for link l. We also assume that the process remains wide-sense stationary for a short period of time. These assumptions allow the recent variance of the process to be estimated from a history buffer of the previous N_B samples for each link. The short-term unbiased sample variance $\hat{s}_l$ for each link l is computed by

$$\hat{s}_l = \frac{1}{N_B - 1} \sum_{p=0}^{N_B - 1} (R_l[k - p] - \bar{R}_l[k])^2, \quad (14)$$

where

$$\bar{R}_l[k] = \frac{1}{N_B} \sum_{p=0}^{N_B - 1} R_l[k - p] \quad (15)$$

is the mean of the signal strength buffer. The sample variance vector for all links in the wireless network is

$$\hat{\mathbf{s}} = [\hat{s}_1, \hat{s}_2, \ldots, \hat{s}_M]^T. \qquad (16)$$

3.6 Regularization and Image Estimation

The linear model (4) provides a mathematical framework relating movement in space to a link's RSS variance. The model is an ill-posed inverse problem that is highly sensitive to measurement and modeling noise. No unique solution to the least-squares formulation exists, and regularization must be applied to obtain a solution. In this paper, *Tikhonov* regularization is used, but other common forms of regularization as they apply to RTI are discussed and evaluated in [25].

In Tikhonov least-squares regularization, the optimization for image estimation is formulated as

$$\mathbf{x}_{Tik} = \arg\min_{\mathbf{x}} \frac{1}{2}\|\mathbf{W}\mathbf{x} - \hat{\mathbf{s}}\|^2 + \alpha\|\mathbf{Q}\mathbf{x}\|^2, \qquad (17)$$

where $\mathbf{Q}$ is the *Tikhonov matrix* that enforces a solution with certain desired properties, and α is a tunable regularization parameter. Taking the derivative of (17) and setting to zero results in the solution:

$$\mathbf{x}_{Tik} = (\mathbf{W}^T\mathbf{W} + \alpha\mathbf{Q}^T\mathbf{Q})^{-1}\mathbf{W}^T\mathbf{s}. \qquad (18)$$

Tikhonov regularization provides a simple framework for incorporating desired characteristics into the VRTI reconstruction. If smooth images are desired, a difference matrix approximating the derivative of the image can be used as the Tikhonov matrix. If the image is 2D, the regularization should include the difference operations in both the vertical and horizontal directions. Let $\mathbf{D}_x$ be the difference operator for the horizontal direction, and $\mathbf{D}_y$ be the difference operator for the vertical direction. Then, the Tikhonov regularized least-squares solution is

$$\mathbf{x}_{Tik} = \Pi\hat{\mathbf{s}}$$
$$\Pi = [\mathbf{W}^T\mathbf{W} + \alpha(\mathbf{D}_x^T\mathbf{D}_x + \mathbf{D}_y^T\mathbf{D}_y)]^{-1}\mathbf{W}^T. \qquad (19)$$

In summary, the variance of each link is estimated from a recent history of RSS samples and stored in vector $\hat{\mathbf{s}}$. The regularized image solution is simply a linear transformation Π of this vector $\hat{\mathbf{s}}$.

4 KALMAN FILTER TRACKING

A radio tomography image in itself does not provide the location coordinates of moving objects. The Kalman filter provides a framework to track such coordinate estimates. Kalman filters are used extensively to estimate the hidden state of a system when measurements of that state are linear and have been corrupted by Gaussian noise. It takes into account the current and previous measurements to generate a more accurate estimate of the system's state than a single instantaneous measurement can. A Kalman filter also has the desirable characteristic that the estimate can be updated with each new measurement, without the need to perform batch measurement collection and processing.

In a location tracking system, such as the one described in this paper, the state to be estimated is made up of the

physical coordinates of the object being tracked. The Kalman filter exploits the fact that an object moves through space at a limited speed, smoothing the effects of noise and preventing the tracking from "jumping." In this sense, the filter can be viewed as a form of regularization.

In this work, the objects being tracked are assumed to move as a Brownian process, and measurement noise is assumed to be Gaussian. Although these assumptions are not entirely accurate, the Kalman filter is still effective for tracking the location of movement. The following variables are used in the tracking filter:

- v_m^2: the variance of the object's motion process, indicating how fast the object is capable of moving. Larger values enable the filter to track faster moving objects, but also make the estimate noisier.
- v_n^2: the variance of the measurement noise. Larger values will cause the filter to "trust" the statistical predictions over the instantaneous measurements.

With these assumptions and variables, the Kalman filter algorithm for tracking movements in an RTI system can be described by the following steps:

1. Initialize $\mathbf{c} = (0, 0)$ and $\mathbf{P} = \mathbf{I}_2$, where $\mathbf{I}_2$ is the 2×2 identity matrix.
2. Set $\bar{\mathbf{P}} = \mathbf{P} + v_m^2\mathbf{I}_2$.
3. Set $\mathbf{G} = \bar{\mathbf{P}}(\bar{\mathbf{P}} + v_n^2\mathbf{I}_2)^{-1}$.
4. Take measurement $\mathbf{z}$ equal to the coordinates of the maximum of the VRTI image.
5. Set $\mathbf{c} = \mathbf{c} + \mathbf{G}(\mathbf{z} - \mathbf{c})$.
6. Set $\mathbf{P} = (\mathbf{I}_2 - \mathbf{G})\bar{\mathbf{P}}$.
7. Jump back to step 2 and repeat.

For information on the derivation of this algorithm, there are many textbooks on the topic of Kalman filtering [26], [27].

5 EXPERIMENT

5.1 Description and Layout

This section presents the results of a through-wall tracking experiment utilizing variance-based RTI. A 34-node peer-to-peer network was deployed in an area around a four-wall portion of a typical home. Three of the walls are external, and one is located on the interior of the home. The interior wall is made of brick and was an external wall prior to remodeling of the home. Objects like furniture, appliances, and window screens were not removed from the home to ensure that the tracking was functional in a natural environment.

The nodes were placed in a rectangular perimeter, as depicted in Fig. 2. It was neither possible, nor necessary, to place the nodes in a uniform spacing due to building and property obstacles. Eight of the nodes were placed on the inside of the building, but on the other side of the brick interior wall. Each radio was placed on a stand to keep them on the same 2D plane at approximately human torso level.

The nodes utilize the IEEE 802.15.4 protocol, and transmit in the 2.4 GHz frequency band. To avoid network transmission collisions, a simple token passing protocol is used. Each node is assigned an ID number and programmed with a known order of transmission. When a node transmits, each
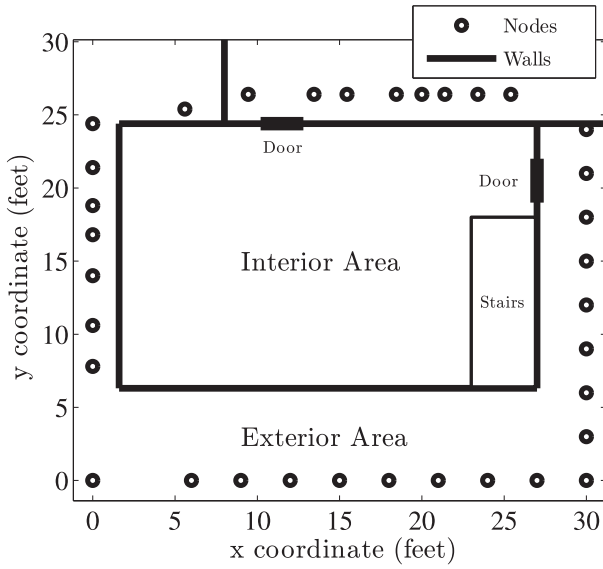
Fig. 2. The layout of a 34-node variance-based RTI through-wall tracking experiment.
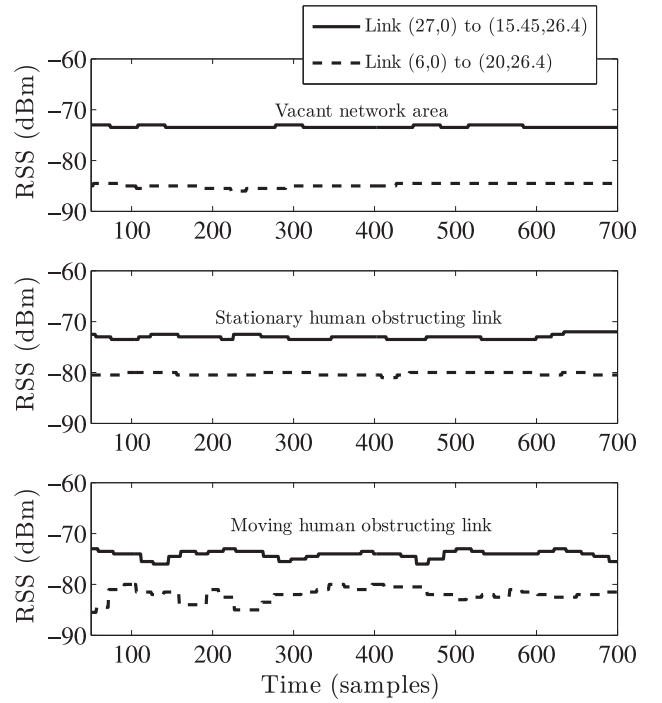

Fig. 3. RSS measurements for two links in a through-wall wireless network. Comparison of these signals illustrates the advantage of using variance over mean for through-wall imaging of human motion.

node that receives the transmission examines the sender identification number. The receiving nodes check to see if it is their turn to transmit, and if not, they wait for the next node to transmit. If the next node does not transmit, or the packet is corrupted, a timeout causes each receiver to move to the next node in the schedule so that the cycle is not halted. A base-station node that receives all broadcasts is used to gather signal strength information and save it to a laptop computer for real-time processing.

In all the experimental results in this section, the same set of image reconstruction parameters is used, as shown in Table 1.

Shadowing-based RTI [1] uses the difference in average signal strength to image the attenuation caused by objects in a wireless network. In through-wall imaging, however, the effect of dense walls prevent many of the links from experiencing significant path loss due to a single human obstructing the link. In many cases, multipath fading can cause the signal strength to increase when a human obstructs a link.

Variance can be used as an indicator of motion, regardless of the average path loss that occurs due to dense walls and stationary objects within the network. An example of how through-wall links are affected by obstruction is provided in Fig. 3. When a stationary object obstructs the link in a through-wall environment, the change in mean RSS is unpredictable. For example, in Fig. 3, one link appears unaffected by the obstruction, while another link's RSS average is raised by approximately 4 dB. When an

object moves, the variance of the obstructed link's RSS provides a more reliable metric, as seen in the figure.

5.2 Image Results

To further demonstrate the advantage of using VRTI over shadowing-based RTI for through-wall motion imaging, two images are presented in Fig. 4. In both images, a human moves randomly, taking small steps around and through the space directly above the coordinate. This is necessary since VRTI images movement, not static changes in attenuation.

Inspection of Fig. 4 shows that VRTI is capable of imaging areas of motion behind walls, while conventional RTI fails to image the change in attenuation. These results are typical of other location coordinates tested during the experiment.

Tracking multiple moving targets through dense walls is a challenging and open topic for future research. When multiple people move within a surveillance area, the accuracy of a VRTI image is dependent on the separation of the targets. Additionally, when multiple walls or walls constructed with dense materials surround the surveillance area, the amount of power that radiates into the area is reduced. Systems attempting to track movement in these difficult circumstances may require low radio frequencies and directional antennas to achieve usable results.

5.3 Path Tracking

In this section, we test our tracking system with experimental data. An experimenter moves at a typical walking pace on a predefined path at a constant speed. A metronome and uniformly placed markings on the floor help the experimenter to take constant-sized steps at a regular time interval.

TABLE 1
VRTI Image Reconstruction Parameters

Parameter	Value	Description
Δ_p	1.5	Pixel width (ft)
λ	.1	Width parameter of weighting ellipse (ft)
α	100	Regularization parameter
ψ	60	Variance weighting scale (dB)^2
N_B	50	Length of RSS buffer

(a)   (b)
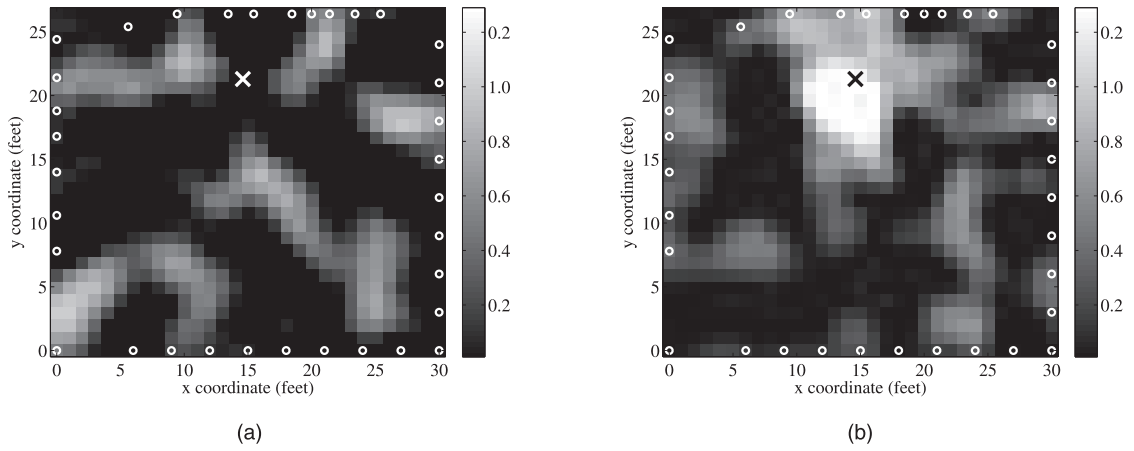
Fig. 4. Comparison of shadowing and variance-based RTI results for through-wall imaging. The experimenter is moving at coordinate (14.6,21.3) in both of these images. (a) Shadowing-based RTI. (b) Variance-based RTI.
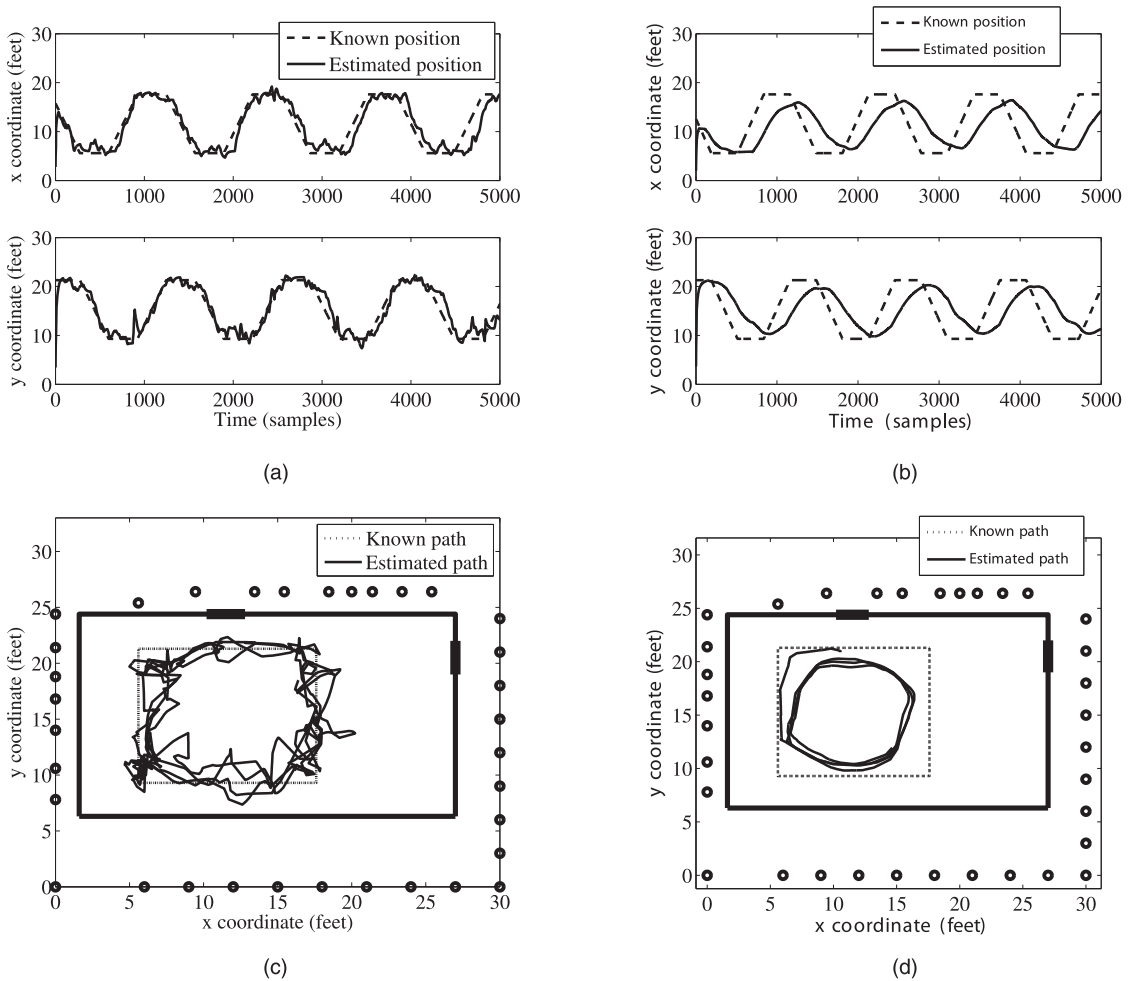

(a)   (b)

(c)   (d)

Fig. 5. The location of human movement moving along a known rectangular path is estimated using varying v_m and constant $v_n^2 = 5$. In (a) and (c), the mobility is set empirically to track objects moving at a few feet per second. In (b) and (d), the mobility is set too low, causing the tracking filter to lag excessively. (a) $v_m^2 = 0.01$ and $v_n^2 = 5$. Average error $\epsilon = 2.07$ feet, (b) $v_m^2 = 0.0001$ and $v_n^2 = 5$. Average error $\epsilon = 5.44$ feet, (c) $v_m^2 = 0.01$ and $v_n^2 = 5$. Average error $\epsilon = 2.07$ feet, (d) $v_m^2 = 0.0001$ and $v_n^2 = 5$. Average error $\epsilon = 5.44$ feet.

The experimenter's actual location is interpolated using the start and stop time, and the known marker positions.

The location of the experimenter is estimated using the Kalman filter described in Section 4 with imaging parameters presented in Table 1. Fig. 5 plots both the known and estimated location coordinates over time when using two different mobility parameters.

The effect of the tracking parameters is visually evident in Fig. 5. When the mobility parameter is set high, the filter is able to track the human with less lag, but the variance of the estimate also increases. When the mobility parameter is set low, the tracking coordinate severely lags behind the moving object, but estimates a smoother path of motion.
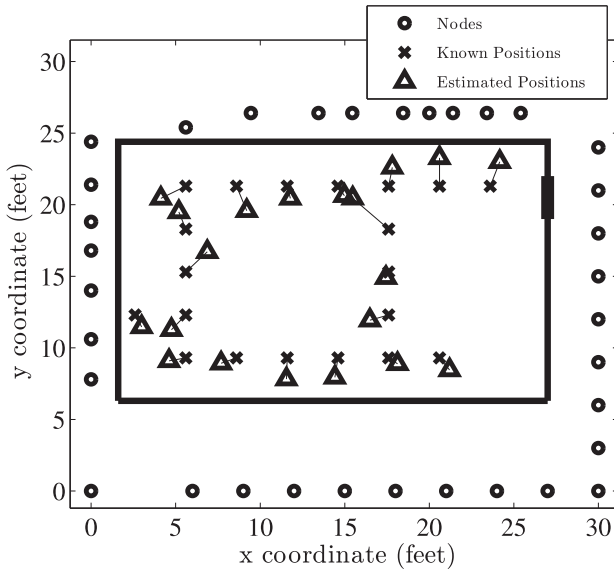
Fig. 6. The ten second average locations of human movement over 20 known positions is estimated using VRTI and Kalman filter tracking with parameters $v_m^2 = 0.01$ and $v_n^2 = 5$. The average error for this experiment $\zeta = 1.46$ feet.

To quantify the accuracy of the location coordinate estimation, the average error is defined as

$$\epsilon = \frac{1}{L}\sum_{k=1}^{L}\sqrt{(z_x[k] - p_x[k])^2 + (z_y[k] - p_y[k])^2}, \qquad (20)$$

where L is the total number of samples, $z_x[k]$ and $z_y[k]$ are the estimated x and y coordinates at sample time k, and $p_x[k]$ and $p_y[k]$ are the actual known coordinates. The average tracking error for $v_m^2 = 0.01$ and $v_n^2 = 5$ is 2.07 feet.

It should be noted that a Kalman filter can be designed to estimate the target's velocity, as well as position. This would enable the filter to follow a nonaccelerating moving object without a lag. However, when a target changes direction or speed, some transient error would occur while the filter converges to the new speed and direction.

5.4 Spot Movement

When estimating the location of a moving object, some amount of tracking lag must occur due to the time it takes to collect measurements from the network and the processing delays. The lag is also dependent on the mobility parameter v_m used for tracking.

To study the tracking system without the effects of time delay, the estimated and known location of a moving human are compared at 20 different coordinates. At each location, the experimenter moves randomly, taking small steps around and through the space directly above the known coordinate. The VRTI tracking system estimates the location of movement and we average the estimates over a duration of ten seconds for each coordinate. The average estimated coordinate is plotted with the known location to generate the results presented in Fig. 6.

To quantify the accuracy in this test, the error for each of the 20 known coordinates is averaged

$$\zeta = \frac{1}{20}\sum_{p=1}^{20}\epsilon_p, \qquad (21)$$

where ϵ_p is the average error defined by (20) for each position p. The error for this test with $v_m^2 = 0.01$ and $v_n^2 = 5$ is 1.46 feet.

5.5 Effect of Imaging Parameters on Tracking Accuracy

The RTI parameters shown in Table 1 must be chosen appropriately, as they affect the accuracy of tracking. The elliptical width parameter λ, regularization parameter α, and buffer size N_B are especially important, as the other parameters for pixel size and scaling are mostly arbitrary.

The elliptical width parameter λ is important to minimize modeling error and maximize tracking performance. If the weighting ellipse is set too large, motion from objects within the ellipsoid will not contribute significantly to the variance of the corresponding link, and contrast in the VRTI result will be lost. If the ellipse is set too narrow, motion outside the ellipsoid will contribute significantly to the pixels that are inside, resulting in images with many false bright spots. Fig. 7a shows the average tracking error ϵ in feet for three buffer sizes over a range of elliptical width parameter values. In this experiment, the most accurate tracking was accomplished with λ set to approximately 0.1.

The amount of regularization applied to the imaging can significantly affect the accuracy of tracking. If regularization is set too low, sharp noise will corrupt the images and cause the tracking mechanism to jump to erroneous locations. If the images are overregularized, the images become too flat and smooth, causing the tracking mechanism to drift in a large circle around the target position. Fig. 7b shows the average tracking error ϵ in feet for three buffer sizes over a range of regularization parameter values. In this experiment, the most accurate tracking was accomplished with $\alpha = 100$.

The variance buffer size plays an important role in tracking accuracy. When N_B is very low, a very small amount of data is used for the variance calculation and the VRTI images are highly susceptible to noise and modeling error. When the buffer sizes are too large, the VRTI images are blurred by the motion of the targets, and tracking lag increases. The most accurate tracking is achieved when there is a balance of the two extremes. Fig. 7c shows the average tracking error ϵ in feet for three regularization values over a range variance buffer values. In this experiment, the most accurate tracking was accomplished with buffer size $N_B = 50$.

6 FUTURE RESEARCH

Many areas of future research are possible to improve VRTI through-wall tracking technology. First, improvements to the multipath models will allow a system to track multiple individuals more accurately, and with less nodes. Many of the assumptions presented in this paper are accurate only for cases where motion images are sparse. More accurate statistical models of the multipath channel for device-free localization will be needed to track multiple people that move in close proximity.

Wireless protocol research is another important part of the improvement of VRTI. Large and scalable networks capable of tracking entire homes and buildings need to be
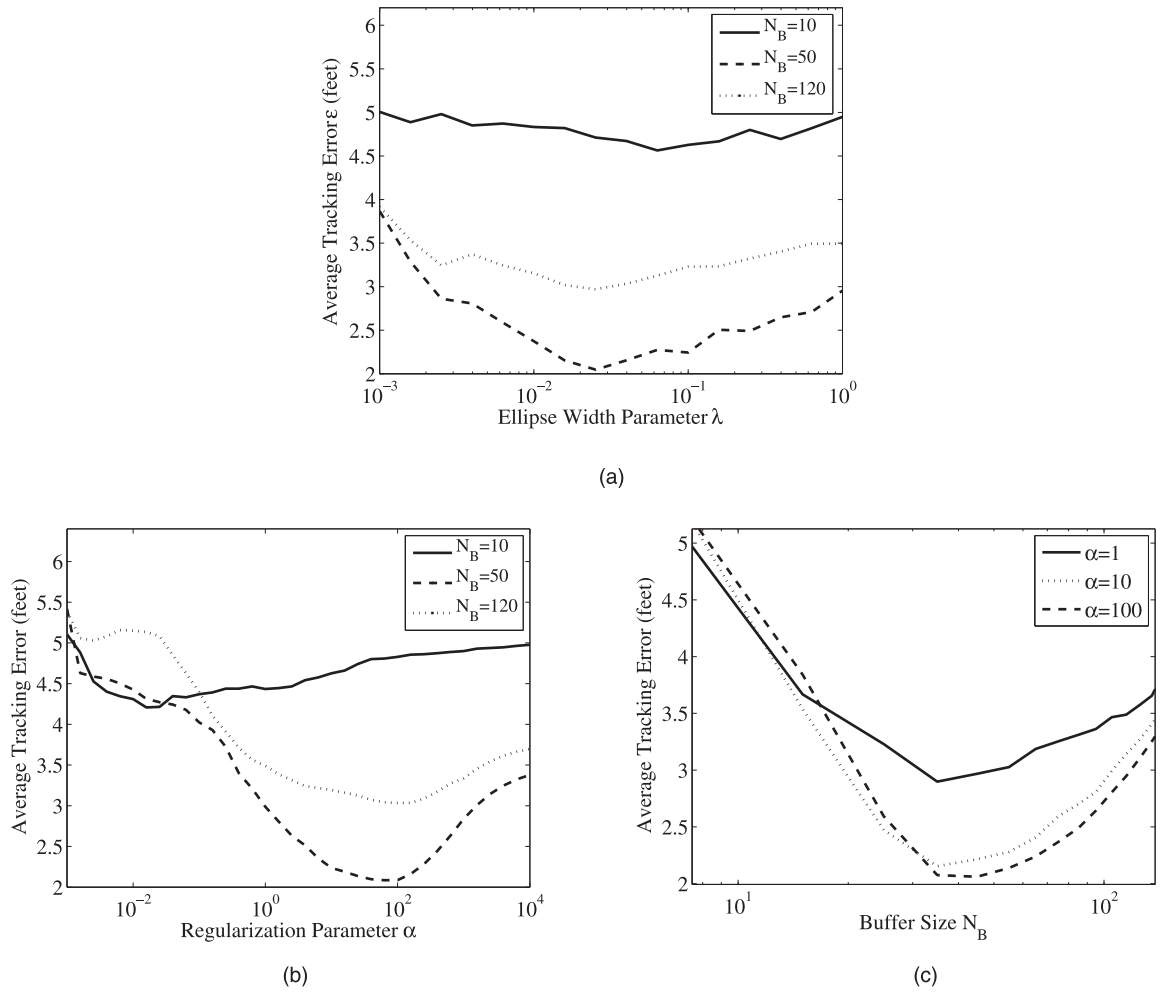
Fig. 7. Average tracking error ϵ in feet for various VRTI parameters. Other parameters are equal to those shown in Table 1. (a) Effect of ellipse width parameter λ. (b) Effect of regularization parameter α. (c) Effect of buffer size N_B.

explored. This will require advanced wireless networking protocols that can measure the RSS of each link quickly when the number of nodes is high. Perhaps frequency hopping and grouping of nodes will allow a VRTI system to measure each link's RSS while maintaining a low delay in delivering the measurements to a base station.

Advancements on the physical layer modeling will allow VRTI systems to track movement more accurately, and with less nodes. In this paper, an ellipsoid model is used to relate RSS variance on a link to the locations of movements. This is certainly an approximation, and future work will require the refinement of the variance weighting model, thus leading to more accurate motion images and coordinate tracking. Other regularization and image estimation techniques may also improve through-wall tracking.

Radio devices could be designed specifically for VRTI tracking applications. The affect of overall node transmission power on imaging performance is an important area to be investigated. Directional and dual-polarized antenna designs would most likely improve images in a through-wall VRTI system. Radio devices capable of sticking to an exterior wall and directively transmitting power into the structure would be extremely useful in emergency deployment and multistory VRTI.

Finally, localization of nodes plays a significant role in tracking of motion with VRTI networks. In an emergency, rescue or enforcement teams will not have time to survey a location. With automatic node self-localization techniques, the nodes could be thrown or randomly placed around an area without measurement, thus saving valuable time.

7   CONCLUSION

Locating interior movement from the outside of a building is extremely valuable because it enables police, military forces, and rescue teams to make life-saving decisions. Variance-based radio tomography is a powerful new method for through-wall imaging that can be used to track the coordinates of moving objects. The cost of VRTI hardware is very low in comparison to existing through-wall imaging systems, and a single network is capable of tracking large areas. These features may enable many new applications that are otherwise impractical.

This paper discusses how RSS variance relates to the power contained in multipath components affected by moving objects. The variance of RSS is related to the location of movement relative to node locations, and this paper provides a formulation to estimate a motion image based on variance measurements. The Kalman filter is

applied as a mechanism for tracking movement coordinates from image data. A 34-node VRTI experiment is shown to be capable of tracking a moving object through typical home exterior walls with an approximately two foot average error. An object moving in place can be located with approximately 1.5 ft average error.

The experiments presented in this paper demonstrate the theoretical and practical capabilities of VRTI for tracking motion behind walls. Many avenues for future research are presented which may improve image accuracy and enable larger and faster VRTI networks. These future research areas include wireless protocols, antenna design, radio channel modeling, localization, and image reconstruction.

ACKNOWLEDGMENTS

REFERENCES

[1] J. Wilson and N. Patwari, "Radio Tomographic Imaging with Wireless Networks," *IEEE Trans. Mobile Computing,* vol. 9, no. 5, pp. 621-632, Jan. 2010.

[2] M. Youssef, M. Mah, and A. Agrawala, "Challenges: Device-Free Passive Localization for Wireless Environments," *Proc. ACM MobiCom,* pp. 222-229, Sept. 2007.

[3] A. Dey and G. Abowd, "Towards a Better Understanding of Context and Context-Awareness," *Proc. CHI Workshop on the What, Who, Where, When, and How of Context-Awareness,* pp. 304-307, 2000.

[4] R. Want, A. Hopper, and V. Gibbons, "The Active Badge Location System," *ACM Trans. Information Systems,* vol. 10, no. 1, pp. 91-102, 1992.

[5] A. Hunt, C. Tillery, and N. Wild, "Through-the-Wall Surveillance Technologies," *Corrections Today,* vol. 63, July 2001.

[6] R.J. Bultitude, "Measurement, Characterization, and Modeling of Indoor 800/900 MHz Radio Channels for Digital Communications," *IEEE Comm. Magazine,* vol. 25, no. 6, pp. 5-12, June 1987.

[7] K. Woyach, D. Puccinelli, and M. Haenggi, "Sensorless Sensing in Wireless Networks: Implementation and Measurements," *Proc. Second Int'l Workshop Wireless Network Measurement (WinMee '06),* 2006.

[8] T. Pratt, S. Nguyen, and B. Walkenhorst, "Dual-Polarized Architectures for Sensing with Wireless Communications Signals," *Proc. IEEE Military Comm. Conf. (MILCOM '08),* pp. 1-6, 2008.

[9] F. Aryanfar and K. Sarabandi, "Through Wall Imaging at Microwave Frequencies Using Space-Time Focusing," *Proc. IEEE Antennas and Propagation Soc. Int'l Symp. (APS '04),* vol. 3, pp. 3063-3066, June 2004.

[10] A. Lin and H. Ling, "Through-Wall Measurements of a Doppler and Direction-of-Arrival (DDOA) Radar for Tracking Indoor Movers," *Proc. IEEE Antennas and Propagation Soc. Int'l Symp. (APS '05),* vol. 3B, pp. 322-325, July 2005.

[11] M. Lin, Z. Zhongzhao, and T. Xuezhi, "A Novel Through-Wall Imaging Method Using Ultra Wideband Pulse System," *Proc. IEEE Int'l Conf. Intelligent Information Hiding and Multimedia Signal Processing,* pp. 147-150, June 2006.

[12] L.-P. Song, C. Yu, and Q.H. Liu, "Through-Wall Imaging (TWI) by Radar: 2D Tomographic Results and Analyses," *IEEE Trans. Geoscience and Remote Sensing,* vol. 43, no. 12, pp. 2793-2798, Dec. 2005.

[13] A. Vertiy, S. Gavrilov, V. Stepanyuk, and I. Voynovskyy, "Through-Wall and Wall Microwave Tomography Imaging," *IEEE Antennas and Propagation Soc. Int'l Symp. (APS '04),* vol. 3, pp. 3087-3090, June 2004.

[14] "Cambridge Consultants," http://www.cambridgeconsultants.com, 2009.

[15] "Camero Tech," http://camero-tech.com, 2010.

[16] A.R. Hunt, "Image Formation through Walls Using a Distributed Radar Sensor Network," *Proc. SPIE Conf. Sensors, and Command, Control, Comm., and Intelligence (C3I) Technologies for Homeland Security and Homeland Defense IV,* pp. 169-174, May 2005.

[17] A.M. Haimovich and R.S. Blum, L.J. Cimini, Jr, "MIMO Radar with Widely Separated Antennas," *IEEE Signal Processing Magazine,* vol. 25, no. 1, pp. 116-129, Jan. 2008.

[18] E. Fishler, A. Haimovich, R. Blum, L. Ciminio, D. Chizhik, and R. Valenzuela, "Spatial Diversity in Radars—Models and Detection Performance," *IEEE Trans. Signal Processing,* vol. 54, no. 3, pp. 823-838, Mar. 2006.

[19] G.D. Durgin, T.S. Rappaport, and D.A. de Wolf, "New Analytical Models and Probability Density Functions for Fading in Wireless Communications," *IEEE Trans. Comm.,* vol. 50, no. 6, pp. 1005-1015, June 2002.

[20] D. Tse and P. Viswanath, *Fundamentals of Wireless Communication.* Cambridge Univ., 2005.

[21] S. Haykin and M. Moher, *Modern Wireless Communications.* Pearson Prentice Hall, 2005.

[22] P. Agrawal and N. Patwari, "Correlated Link Shadow Fading in Multi-Hop Wireless Networks," vol. 8, no. 8, *IEEE Trans. Wireless Comm.,* Aug. 2009.

[23] D. Zhang, J. Ma, Q. Chen, and L. Ni, "An RF-Based System for Tracking Transceiver-Free Objects," *Proc. Fifth Ann. IEEE Int'l Conf. Pervasive Computing and Comm. (PerCom '07),* pp. 135-144, 2007.

[24] D. Zhang and L. Ni, "Dynamic Clustering for Tracking Multiple Transceiver-Free Objects," *Proc. IEEE Int'l Conf. Pervasive Computing and Comm. (PerCom '09),* pp. 1-8, 2009.

[25] J. Wilson and N. Patwari, "Regularization Methods for Radio Tomographic Imaging," *Proc. Virginia Tech Symp. Wireless Personal Comm.,* June 2009.

[26] P.S. Maybeck, *Stochastic Models, Estimation, and Control.* Academic, 1979.

[27] G. Welch and G. Bishop, "An Introduction to the Kalman Filter," Univ. of North Carolina at Chapel Hill, 1995.

Joey Wilson received the PhD degree from the Department of Electrical and Computer Engineering, University of Utah, in 2010. He is the founder and president of Xandem Technology, a company dedicated to radio tomography and wireless network device-free sensing technologies. His research interests include signal processing, estimation and detection theory, and communications. Prior to his doctorate studies, Dr. Wilson worked in research and development at L-3 Communications (Communications Systems West) in Salt Lake City from 2004 to 2008.

Neal Patwari received the BS and MS degrees in electrical engineering from the Virginia Polytechnic Institute and State University in 1997 and 1999, respectively, and the PhD degree in electrical engineering from the University of Michigan in 2005. Currently, he is working as an assistant professor in the Department of Electrical and Computer Engineering, University of Utah, with an adjunct appointment in the School of Computing. He was a research engineer with Motorola Labs, Florida, between 1999 and 2001. He directs the Sensing and Processing Across Networks (SPAN) Lab, which performs research at the intersection of statistical signal processing and wireless networking. His research interests are in radio channel signal processing, in which radio channel measurements are used for purposes of security, localization, and networking. He has served on technical program committees for conferences such as SECON, ICDCS, DCOSS, ICCCN, ICC, and MILCOM, and is the publicity chair for IPSN 2010. He is an associate editor of the *IEEE Transactions on Mobile Computing.* He is a member of the IEEE.

▷ **For more information on this or any other computing topic, please visit our Digital Library at** www.computer.org/publications/dlib.